Modelling geochemical and kinetic processes involved in lead (Pb) remobilization during resuspension events of contaminated sediments.

Philippe Ciffroy, Lucie Monnin, Jean-Marie Garnier, Jean-Paul Ambrosi, Olivier Radakovitch

Modelling geochemical and kinetic processes involved in lead (Pb) remobilization during resuspension events of contaminated sediments

Philippe Ciffroy[1], Lucie Monnin[2], Jean-Marie Garnier[2], Jean-Paul Ambrosi[2], Olivier Radakovitch[2,3]

[1] EDF, Division Recherche et Développement, Laboratoire National d'Hydraulique et Environnement (LNHE), Chatou, France.

[2] Aix Marseille Univ, CNRS, IRD, INRA, Coll France, CEREGE, Aix-en-Provence, France

[3] Institut de Radioprotection et de Sûreté Nucléaire (IRSN), PSE-ENV/SRTE/LRTA, BP3, 13115 Saint-Paul Lez Durance, France

Abstract

The objective of this paper is to present a model simulating and predicting the exchange kinetics of lead (Pb) between contaminated sediments and water during resuspension events potentially occurring in reservoirs. We developed an innovative model that combines thermodynamic speciation of particulate surfaces (oxides and POC), thermodynamic Pb speciation in water, and kinetic modelling of exchanges between free Pb and particulate sites (i.e. dissolution of a carbonate carrier phase, adsorption/coprecipitation and desorption/dissolution to/from oxides and adsorption and desorption/degradation to/from particulate organic particles). We used results from laboratory resuspension experiments performed on sediments from three contaminated dam reservoirs to calibrate a new chemical speciation model.

Uptake and release processes to/from sediments were found to be controlled by at least two successive reactions that can be associated to two particulate pools (here oxides and POC).

Kinetic adsorption and desorption rates were calibrated for seven experimental conditions. Variability in kinetic rates allowed to evaluate the effect of solid-to-liquid ratio and sediment origin on exchange kinetics at the water-particles interface. It was shown that the kinetic release of dissolved Pb by desorption or dissolution from the oxides is reproduced almost identically between the experiments, regardless of the solid-to-liquid ratio and sediment origin. Readsorption on the long term on POC sites is more variable, even if ranges of variation in the adsorption and desorption kinetic rates related to POC remain limited considering that tested sediments are quite contrasted.

Keywords

Dam reservoir; Metal remobilization; Sediment resuspension; Speciation; Kinetics modeling

Capsule

A kinetic model simulating the dynamics of lead (Pb) during sediment resuspension was developed and calibrated on laboratory experiments performed on three contaminated sediments.

1 Introduction

A large part of the trace metal(loid)s (TM) introduced by anthropogenic inputs in aquatic environments are finally stored in the sediments, where they can be found in two main solid forms: (co)precipitated in mineral forms like sulphides or carbonates, or adsorbed onto the surface of reactive phases like oxyhydroxydes, organic matter or clay. This distribution influences their bioavailability and toxicity, and the extent to which they can be remobilised in the water in case of a change in physicochemical conditions. Indeed, when sediments are

resuspended due to natural events or anthropic activities, the particles undergo a sudden and major change in the pH, redox, solid-to-liquid ratio and other chemical conditions. Resuspension may promote the remobilization of TM from the solid to the dissolved phase (Kalnejais et al., 2010; Superville et al., 2014), and therefore poses a risk of water quality degradation. Remobilization of TM depends both on the characteristics of the sediments, on the TM distribution, and on the physico-chemical conditions prevailing during the resuspension (Cantwell et al., 2002; SedNet, 2014). Besides, TM concentrations that are measured in water during laboratory experiments (e.g. Simpson et al., 2000; Cantwell et al., 2002; Ye et al., 2013; Kalnejais et al., 2010; Hwang et al., 2011) or in-situ resuspension events (Caetano et al., 2003; Superville et al., 2014) result from several kinetic release (desorption/dissolution) and uptake (adsorption/(co)precipitation) processes from/to the suspended particles.

In the case of dams associated with hydroelectric power plants, the reservoirs sometimes need to be fully drawn down for the safety inspections and maintenance tasks (Poupart and Royet, 2010). These draining operations could be a problem in the case of contaminated reservoirs because they lead to sediment resuspension. An increase of dissolved metal concentrations above water quality standards due to remobilization is one of the risks. Being able to estimate it is an important stake in order to improve the management of reservoirs.

Laboratory resuspension experiments are helpful to mimic and predict the remobilization of TM occurring during *in situ* sediment resuspension and to test the influence of particles concentrations or kinetics of chemical reactions. Results of resuspension experiments in numerous works show kinetic evolutions of TM concentrations in the dissolved phase, and competition phenomenon for the adsorption of TM on the solid suspended particles (Saulnier and Mucci, 2000; Caille et al., 2003; Camino Martin-Torre et al., 2017; Monnin et al., 2018). The evolution of TM concentrations in water are thus controlled by both rapid and slow release and uptake processes. Evaluating and predicting the remobilization of TM over time appear thus

important to assess the risk of water quality degradation. These assessments and predictions can be conducted using chemical modelling. Computer codes like Visual Minteq, Phreeqc or WHAM allow to calculate speciation of dissolved TM in waters and the sorption of TM onto solid phases. Most of them cannot however predict the temporal evolution of such distribution, because all the thermodynamic processes included in the codes are assumed to be at equilibrium and the reaction kinetics are not taken into account. Only PHREEQC has the capacity for kinetic modelling using the 'kinetic' and 'rates' keywords; the Geochemist's Workbench (www.gwb.com) also has kinetic capabilities for metal(loid) speciation reactions, but they need to be defined in the software by the modeler.

Taking into account this background, we first developed a new chemical speciation model combining thermodynamic and kinetic processes; this model simulates exchange reactions between free dissolved TMs and solid surfaces and is theoretically applicable to all TMs. We then used results from laboratory 'long-term' resuspension experiments performed on sediments from three contaminated dam reservoirs to calibrate this model for a specific TM as an example, i.e. lead (Pb). On a modelling point of view, Pb speciation, adsorption/precipitation and desorption/dissolution is used here as a proxy for trace metals in a very general way. However, it can obviously not be used as a proxy in a quantitative way. Moreover, it cannot be used as a proxy for metalloids such as As and Se, as their behavior is very different from the divalent trace metal cations. It should be noted here that the notions of 'short-' vs 'medium-' vs 'long term' experiments are quite relative and must be put in perspective with the purpose of the study. In our case, the purpose of the study was to investigate fate of TMs during management operations on dams that occur during some hours. So, the 'long-term' terminology is consistent with the duration of our experiments (i.e. 160 hours). Our objective was then to combine a thermodynamic model with a kinetic model simulating exchange reactions between free dissolved metal and solid surfaces. This model, coded under the Ecolego® platform (Nia et al.,

2011; Ciffroy et al., 2011, 2016), is based on processes similar to those included in e.g. Visual Minteq, but it allows the user to describe sorption/desorption reactions by their kinetic rates, instead than by their equilibrium affinity constants. Ecolego® was selected as the coding platform because it is a systems oriented software program instead of geochemical modelling software like PHREEQC. Moreover, it is designed for uncertainty and sensitivity analysis and such capabilities can be of concern for future applications (Ciffroy and Benedetti, 2018). This paper presents the fundamental of this model and focus on the behavior of one major TM as an example, i.e. lead (Pb).

2 Material and methods

This section describes the experimental design used for collecting site-specific data and the model approach developed for describing kinetics in the exchange of TM between water and particles.

2.1 Study site, sampling and sediment characterization

Sediments were sampled from three French reservoirs, operated for hydroelectricity: Les Mesches, Queuille and Rochebut, denoted hereafter A, B and C (Figure 1).

Reservoir A has a surface of 9.5 ha and is located in the south of the French Alps. High levels of As, Cd, Pb and Zn were found in the sediments due to the presence of two ancient Pb-Zn mines in the watershed. The zinc and lead sulphides ores were exploited from 1750 to 1927. The origin of these TM is unambiguous regarding the small size of the watershed and the fact that it was not occupied by humans except for the mine extraction.

Reservoir B is located in the French Massif Central, 30 km northwest of the city of Clermont-Ferrand. Reservoir B has a surface of 36 ha and a maximal depth of about 30 m. A number of

former mining sites of Pb, As and F exist in the watershed, and in particular several deposits of
110 Ag and Pb were exploited in this mining zone.

Reservoir C is located in the French Massif Central. Gold was intensively mined in the area in
112 the twentieth century and the exploitation generated 300 000 m^3 of tailings disposed on a 5 hectare site (rehabilitated in 2010-2011), in close proximity of the river about 12 km upstream
114 from the reservoir.

Water and sediment were collected in June 2015 in the reservoir A and in April 2016 in the
116 reservoirs B and C. Water was pumped out from the shore and passed through a ceramic filter of 0.4 µm. Sediment samples (0-10 cm surface layer) were collected with an interface UWITEC®
118 corer. The sediment was directly extracted to measure Eh and pH (by planting the electrodes in the wet sediment), and placed into sealed glass jars to maintain their reduced state. It was
120 manually homogenized in the laboratory in a N_2 filled glove-bag, and divided into several sub-samples that were stored in individual glass jars at 4°C in darkness. A new jar was opened for
122 each resuspension experiment, and Eh and pH were measured to check the good conservation of the sediments. They were compared with those measured during the sampling to check the good
124 conservation of the sediments.

All the methods that were undertaken for characterizing the sediment were described in detail in
126 Monnin et al (2018).

128 **2.2 Lead (Pb) distribution in sediment**

For running the model described hereafter it is necessary to define initial conditions, i.e. the
130 concentrations of Pb in each of the particulate phases (oxides, Particulate Organic Carbon (POC), precipitated carbonates) at the initial time of the resuspension experiments. These initial
132 conditions were determined experimentally with ascorbate and sequential extractions. The

ascorbate extractions were carried out to quantify more specifically the trace metals bound to amorphous and easily reducible Fe and Mn oxides and hydroxydes. Ferrihydrite and iron monosulfide (FeS) are considered soluble in the ascorbate solution, in contrary to pyrite, hematite or goethite (Ferdelman, 1988; Kostka et Luther, 1994; Anschutz et al., 1998). The standardized BCR 3-step extraction scheme (Rauret, 1998; Quevauviller, 2007) was slightly modified in order to adapt the one of Tessier et al. (1979) to the first fraction and to separate the "exchangeable" and "carbonate" fractions. The sequential extraction provides then four fractions: exchangeable (F1a); carbonates-bound metals (F1b); reducible fraction (F2 from BCR) and the oxidizable fraction (F3 from BCR). The detailed procedure is described in Monnin et al (2018). Finally, the residual fraction is assumed to be equal to the total metal content minus the sum of the previous four fractions. The Pb fraction that could be extracted simultaneously with Acid Volatile Sulphides (AVS) was not evaluated because the redox potentials in the sediments (+245 mV for reservoir A and +270-290 mV for reservoir B and C) do not favour the occurrence of AVS phases (De Jonge et al, 2012).

Procedures followed for conducting the chemical extractions are described in detail in Monnin et al.(2018).

2.3 Laboratory resuspension experiments

Aliquots of sediments were resuspended using an Applikon® bioreactor, a 3L glass reactor in which the sediment is stirred by both a propellers assembly and a magnetic stirrer. pH, Eh, dissolved oxygen and temperature were measured continuously with four probes passed through the head plate on the top of the reactor (Monnin et al., 2018).

Each resuspension experiment was performed on a new sample from a sealed jar. A mass of wet sediment was inserted into the 3L reactor filled with filtered water collected from the respective sampling site. Ambient air was continuously bubbled into the reactor to mimic the real environmental situation of a draining operation. A total of seven experiments were conducted,

158 with sediment mass corresponding respectively (on a dry sediment to water ratios basis) to 2.7, 5.0 and 9.4 $g.L^{-1}$ for reservoir A, to 1.6 and 5.3 $g.L^{-1}$ for reservoir B and to 2.1 and 4.9 $g.L^{-1}$ for
160 reservoir C. This range of solid-to-liquid ratios was chosen to mimic Suspended Particulate Matter (SPM) concentrations potentially found during draining operations. Such values are
162 realistic when considering experience gained on management of reservoirs. Since hydraulic conditions and shear stress at the vicinity of sediments vary over time during draining operations,
164 SPM concentrations is indeed not constant and may vary at least over one order of magnitude.

The experiments were run for 120 to 160 h. During the experiment, the water was sampled
166 through a syringe inserted into the reactor. 30 mL of water samples were collected successively at the start time (t0) (prior to sediment addition), and again after sediment addition at 2, (5), 10,
168 20, 30 min and 1, 1.5, 2, 5, 15, 24, 48, 72, 96, 120, (160) h. The total volume collected represents a maximum of 18% of the initial water volume in the reactor. Corrections were applied for
170 taking this loss into account. Each sample was separated into three aliquots: a) 10 mL were filtered through 0.7 µm glass microfiber and stored frozen in glass vials until DOC analysis
172 (Shimadzu TOC-V_{CSH} ; PROTEE laboratory); b) 12 mL were filtered through 0.22 µm syringe filters for alkalinity and major ions (Metrohm microtitrator and capillary electrophoresis
174 respectively); c) 8 mL were filtered through 0.22 µm syringe filters and acidified with ultrapur nitric acid for major and trace elements analysis (ICP-MS). A specific resuspension experiment
176 carried out previously to determine the quantity of elements that could be adsorbed onto the glass wall of the reactor showed that this bias is negligible (Monnin et al., 2018).

178

2.4 Conceptual model framework

180 The model developed here is theoretically applicable for all TMs, but the calibration work presented in this paper was dedicated to a specific TM chosen as an example, i.e. lead (Pb). This
182 model is similar to those developed and tested in Ciffroy et al. (2001), Ciffroy et al. (2003) and

Garnier et al. (2006), who studied adsorption and desorption kinetics of TM to/from natural particles collected in the Loire river. For some TM (e.g. Co, Mn, Cs in some conditions), they observed similar kinetic trends as those observed here for Pb (see Results section), i.e. a desorption phase followed by a readsorption phase. They interpreted such experimental results as follows: the TM that desorbed just after mixing corresponds to the TM associated with the weak and fast sites; excess TM in solution are then readsorbed on less accessible and/or more specific sites. From these observations, the authors proposed a 'two-successive reversible' kinetic model that was able to fit the experimental data. This model was adapted here for the purpose of our experimental procedure and results. All the processes, assumptions and parameters involved in the model are summarized in Table 1. Its main principles are described below.

Three particulate phases are here assumed to contribute to TM exchanges between water (dissolved phase) and particles, i.e. oxides, POC and carbonates. The total concentrations of oxides and POC are assumed to be constant over the duration of the experiment. However, physico-chemical conditions like pH or ionic strength showed significant evolution during the experiment (see Results section). As a consequence, speciation of oxides and the POC surface may change over time and such modifications were taken into account in the model.

First, speciation of oxide surfaces (noted hereafter SOH, e.g. FeOH, AlOH and/or MnOH) were modeled. Oxides exhibit an amphoteric behaviour, i.e. they may react with protons (H^+) present in solution to form a net positively charged surface (SOH_2^+) at low pH, or a net negatively charged surface (SO^-) at high pH. Only anionic forms (SO^-) are assumed to interact with cationic free TM in solution. The SO^- fraction was then calculated by a thermodynamic speciation model integrated in our modeling system. For this purpose, we coded the HFO model developed by Dzombak and Morel (1990), which calculates the distribution between SOH, SO^- and SOH_2^+.

Secondly, speciation of the POC surface (noted hereafter *HHS* for protonated Humic Substances) was modeled. Indeed, humic substances may be present as the protonated and deprotonated

208 species *HHS* and HS^-, and cationic TM are assumed to interact with anionic forms (HS^-). The HS^- fraction among the POC surface sites was then calculated by a thermodynamic speciation
210 model integrated in our modeling system. For this purpose, we coded the Stockholm Humic Substances (SHM) model (Gustafsson et al., 2001; Gustafsson et al., 2006), which is similar to
212 WHAM (Tipping, 1998) which calculates the distribution of sites among protonated and deprotonated species.

214 Finally, considering the total dissolved concentration (M_{dis}) would create a bias in the model. Actually, TM species that interact with oxides and POC are not the whole 'dissolved metal' M_{dis},
216 but only its free cationic species M^{z+}. As physico-chemical conditions like pH change over time, the fraction of free species M^{z+} may show variations too. Two kinds of complexation reactions
218 occurring in the dissolved phase were therefore incorporated in our model. On one hand, complexation of TM with inorganic ligands (hydroxides, nitrates, sulfates, chlorine and
220 carbonates) was described by affinity constants at equilibrium K_{ML}. Data are taken from the Visual Minteq database (https://vminteq.lwr.kth.se/). On the other hand, complexation of TM
222 with Dissolved Organic Carbon (DOC), i.e. dissolved humic acids and fulvic acids was described according to the SHM model previously mentioned. It accounts for chemical
224 interactions between DOC and TM, as well as electrostatic interactions at the vicinity of the humic surface.

226 In conclusion, the thermodynamic models integrated in our tool allowed to calculate the fraction of interacting sites on oxides, (SO^-), and on POC, (HS^-), as well as the fraction of free species
228 (f_{free}), for the duration of our experiments. These models are described in detail in Ciffroy and Benedetti (2018).

230 Exchanges are then described by three chemical reactions:

$$f_{free}.M_{dis} + f_{SO^-}.Ox \underset{k_{des,ox}}{\overset{k_{ads,ox}}{\rightleftharpoons}} M_{ox}$$

232

$$f_{free}.M_{dis} + f_{HS^-}.POC \underset{k_{des,POC}}{\overset{k_{ads,POC}}{\rightleftharpoons}} M_{POC}$$

$$f_{free}.M_{dis} \underset{k_{dis,carb}}{\overset{k_{prec,carb}}{\rightleftharpoons}} M_{carb} \searrow$$

234 where M_{dis}, M_{ox}, M_{POC} and M_{carb} represent TM in water, or associated with oxides, POC and precipitated carbonates respectively ($g.L^{-1}$); Ox and POC represent oxides and POC
236 concentrations ($g.L^{-1}$); $k_{ads,ox}$ and $k_{des,ox}$ are the adsorption and desorption kinetic rates (in $L.g_{Ox}^{-1}.h^{-1}$ and h^{-1} respectively) to and from oxides; $k_{ads,POC}$ and $k_{des,POC}$ are the adsorption and
238 desorption kinetic rates (in $L.g_{POC}^{-1}.h^{-1}$ and h^{-1} respectively) to and from POC; $k_{prec,carb}$ and $k_{dis,carb}$ are the precipitation and dissolution kinetic rates (in h^{-1}) to and from carbonates; f_{free} is the
240 fraction of free TM in the dissolved phase (i.e. $\frac{M^{z+}}{M_{dis}}$); f_{SO^-} is the fraction of anionic sites on oxides (i.e. $\frac{SO^-}{SOH+SO^-+SOH_2^+}$); f_{HS^-} is the fraction of anionic sites on POC (i.e. $\frac{HS^-}{HHS+HS^-}$). Actually, transfer
242 of TM from oxides to water can be due to both chemical desorption and solid dissolution. Similarly, transfer of TM from POC to water can be due to both chemical desorption and
244 (a)biotic degradation of the POC. No information is available to distinguish these processes and then the $k_{des,ox}$ and $k_{des,POC}$ parameters implicitly incorporate both desorption and dissolution for
246 oxides, and desorption and degradation for the POC. It will be hereafter called 'desorption'. The same assumption is made for 'adsorption' to oxides and POC that incorporate potential solid
248 formation.

250 **2.5 Initial conditions**

For calibrating the model from experimental results, it is necessary to define the initial
252 conditions of the simulation, i.e. the concentration of Pb in each of the solid phases (i.e. oxides, POC and carbonates) at the start time. Major and trace element concentrations in waters used for

254 the resuspension experiments were measured and were used as initial contents in water.Methods are presented in detail in Monnin et al. (2018) Chemical extractions provide information on
256 element distribution between different solid phases in the sediment before resuspension. The proportion of metals extracted in the fraction F1b with acetic acid $C_2H_4O_2$, and the fraction F3
258 with H_2O_2, in the sequential extraction scheme (Monnin et al., 2018), were respectively used to quantify the metals bound to carbonates and to particulate organic matter. The amount of TM
260 bound to oxides were assumed to be extracted with the ascorbate reagent.

The total amount of oxides in the sediment was derived from the proportions of Fe, Mn and Al in
262 the ascorbate extraction. The proportions of Fe, which is the main component of the oxides, are similar in the ascorbate fraction and in the reducible fraction F2 of the sequential extraction. The
264 Fe-, Mn- and Al- oxides were included in the calculation of the solid oxide phase (Table 2).

266 **2.6 Calibration of dissolution kinetic rate of carbonates**

For each model, the third reaction describes the dissolution of carbonates, leading to a
268 remobilization of associated Pb, and inversely the precipitation of carbonates, leading to a potential co-precipitation of Pb, assuming Pb is in the carbonate fraction. X-ray diffraction
270 showed that calcite ($CaCO_3$) and dolomite ($CaMg(CO_3)_2$) are the major mineral phases the sediments from reservoir A, but magnesian calcite may be also present (Monnin et al., 2018).
272 The proportions of these three phases and their respective contents in TM cannot be calculated. In contrast, calcite was not evidenced in the sediments of reservoir B nor C. For sake of
274 simplicity, calcite was used as a proxy to represent all carbonates . The quantity of calcite in sediment is estimated through the calculation of the Saturation index (*SI*), expressed as:

276 $$SI = \log\left(\frac{IAP}{K_s}\right) \quad (1)$$

where *IAP* is the Ion (Ca^{2+} and CO_3^{2-}) Activity Product; K_s is the solubility product of calcite
278 ($\log_{10}(K_s)$ = -8.48). When the system is undersaturated (i.e. when SI<0), calcite may dissolve and the concentrations of calcium and carbonates may increase. The reaction describing such a
280 dissolution/precipitation process is the following:

$$Ca^{2+} + CO_3^{2-} \underset{k_{dis,carb}}{\overset{k_{prec,carb}}{\rightleftharpoons}} CaCO_3 \downarrow$$

282 As the carbonate concentration (CO_3^{2-}) is also driven by acid/base reactions with HCO_3^- and H_2CO_3, these reactions were also implemented in our model using the pK_a of each reaction and
284 assuming equilibrium.

In the experiments on reservoir A, a significant increase in both Ca^{2+} and CO_3^{2-} concentrations
286 was observed and *SI* is negative, interpreted as a continuous dissolution of calcite. Even if precipitation and dissolution can simultaneously occur, we considered here due to the negative
288 SI that the reaction is predominantly directed as:

$$Ca^{2+} + CO_3^{2-} \xleftarrow{k_{dis,carb}} CaCO_3 \downarrow$$

290 For calibrating the dissolution kinetic rate $k_{dis,carb}$, we used experimental data related to Ca^{2+} and CO_3^{2-}, and subsequent *IAP*. Besides, we experimentally observed that SI follows an exponential
292 trend, so we added an exponential correction factor $\alpha_{dis,carb}$ (unitless) describing the fact that dissolution decreases if SI is close to 0. Kinetic evolution of Ca^{2+} and CO_3^{2-} is then given by:

294 $$\textbf{(2)} \qquad \boldsymbol{If\ SI < 0,} \qquad \frac{d(Ca^{2+})}{dt} = \frac{d(CO_3^{2-})}{dt} = k_{dis,carb} \cdot e^{-\alpha_{dis,carb} \cdot SI}$$

296 We then optimized parameter values to minimize the distance between calculated and measured values according to the procedure described in section 2.8.

298 Pb associated to calcite can be remobilized simultaneously and it is then assumed that the kinetic dissolution rate of calcite-associated Pb is the same as for calcite itself.

300

2.7 Calibration of sorption and desorption kinetic rates to/from oxides/POC

302 Kinetic trends observed for Pb in all our experiments showed two stages, i.e. a first desorption stage followed by a readsorption stage (see Results section). As discussed in Ciffroy et al. 304 (2001), Ciffroy et al. (2003) and Garnier et al. (2006), TM desorbed just after mixing should correspond to TM associated to weak and fast sites, and excess TM in solution are then 306 readsorbed on less accessible and/or more specific sites. From a theoretical point of view, we could then assume that oxides correspond to weak and fast sites, while POC corresponds to 308 strong and slow sites; or vice-versa. When observing adsorption/desorption reactions on oxides and POC, we can observe that oxides and POC play symmetric roles from a mathematical point 310 of view, and that it is mathematically impossible to decide which kind of sites are the weakest and fastest, and which ones are the strongest and slowest.

312 Two scenarios could then be considered from a theoretical point of view. The first one assumes that Pb is weakly associated to oxides and strongly associated to POC. In this scenario, the initial 314 increase of Pb in the solution is predominantly attributed to desorption from oxides and $k_{des,ox} > k_{des,POC}$. This scenario may be supported by a qualitative interpretation of experimental results. 316 Fe and Mn concentrations in water showed indeed a significant increase during the first minutes/hours of the resuspension experiment, suggesting fast processes occurring at the surface 318 of oxides. Besides, Saturation indexes (SI) calculated with Visual MINTEQ indicate undersaturation of several Fe oxides and (oxy)hydroxides (e.g. ferrihydrite, goethite, gibbsite, 320 pyrolusite and manganite) at the beginning of the resuspension experiment, suggesting possible dissolution of oxides (we remind that dissolution and desorption of TM associated to oxides are 322 implicitly confounded in our model). The second scenario assumes that Pb is weakly associated to POC and strongly associated to oxides. In this scenario, the initial increase of Pb in the 324 solution is predominantly attributed to desorption from POC and $k_{des,POC} > k_{des,ox}$. Note also

that potential (a)biotic degradation of POC may occur but is implicitly confounded with desorption in our model.

The choice between these two scenarios was based on the qualitative arguments given above; the first scenario seems reasonable in our study and it was then selected. We then calibrated the kinetic parameters under the constraint $k_{des,ox} > k_{des,POC}$. However, we must keep in mind that this is a prior assumption and not a demonstration.

2.8 Fitting process

The two parameters describing dissolution of carbonates $k_{dis,carb}$ and $\alpha_{dis,carb}$ were first fitted. Then, the four parameters describing exchanges with oxides and POC (i.e. $k_{ads,ox}$, $k_{des,ox}$, $k_{ads,POC}$ and $k_{des,POC}$) were fitted from the experimental results. We conducted a probabilistic approach to define the most probable combinations of parameters, similarly to the process described in Ciffroy et al, 2011 (as illustrated in Figure 2). Instead of determining a single value for each of the parameters, the objective was to define Probability Density Functions (PDF), describing the range of most probable values for each parameter, as well as correlations between parameters. The steps followed for deriving PDFs for each of the model parameters are the following (see fig 1 in Ciffroy et al; 2011):

Step 1: each of the parameters to be fitted is described by a PDF characterizing the range of potential values. As no previous knowledge related to the kinetic rates is available, large log-uniform PDFs (over several orders of magnitude) were first selected. Log-uniform distributions were chosen because they are the less informative ones, allowing to uniformly covering a range of potential values over several orders of magnitude.

Step 2: 10000 values of each parameter were randomly sampled through a Monte Carlo procedure, allowing to obtain 10000 combinations of parameters. The model was run for each of the 10000 combinations of parameters, providing 10000 $M_{dis}=f(t)$ curves.

Step 3: In the experiments described above, variables (i.e. Ca^{2+}, CO_3^{2-} and M_{dis} concentrations) were measured at different deployment times (from 2 minutes to 120 or 160 h, see 2.4). For fitting the parameters related to calcite dissolution, we only used the experimental *SI* values as described above. For fitting the parameters related to TM exchanges with solids, we used the M_{dis} values. Let's write Y the output of interest (i.e. *SI* or M_{dis}). For each of the 10000 simulations previously generated, error was calculated as follows:

$$\varepsilon_p = \sum_i \left(Y_{measured}(t_i) - Y_{p,calculated}(t_i) \right)^2 \quad (3)$$

where $Y_{measured}(t_i)$ and $Y_{p,calculated}(t_i)$ refers to the measured and calculated output at time t_i; the index p refers to the p^{th} combination of parameters (with p=1 to 10000).

Step 4: the 10000 simulations were then ranked according to the error ε_p. The lowest errors ε_p correspond to the 'best' combinations of parameters, i.e. those minimizing the distance between measured and calculated values. To estimate the robustness of the parameterization, it is necessary to estimate the range of parameter values that may give equivalent results. Typically, a non-sensitive parameter will give equivalent errors over a wide range of values, while a sensitive parameter will give equivalent errors over a narrow range of values. To evaluate the set of parameter values that may equivalently give good results, a statistical Wilcoxon test was undertaken on the ranked combinations. Probability Density Functions (PDFs) were thus built for each parameter.

Step 5: once PDFs are fitted for all the parameters, the model is run again replacing the non-informative PDFs used at step 1 (i.e. log-uniform PDFs) by informative PDFs obtained at step 4 (e.g. normal PDFs). Besides, correlations identified between parameters at step 4 are also

introduced in the investigated model. When correlation(s) is(are) defined, the Iman-Conover technique (Iman and Conover, 1982) was processed to generate parameter samples respecting these correlations.

Step 8: calculated curves obtained from the informative PDFs were compared to experimental data. For facilitating the interpretation, this plot is synthesized by three curves, i.e. the curve obtained with the best combination of parameters, and the 5^{th} percentile and 95^{th} percentile curves respectively.

The fitting process described above was performed for each of the seven experimental conditions. We thus obtained parameter PDFs for each of these seven experiments and the consistency of these PDFs among sites and solid-to-liquid ratios was discussed (see section 3.5). Another approach to calibration was also tested to discuss the model's capabilities: parameter PDFs were calibrated by considering all the experiments performed for site A together (site A was chosen for this calibration exercise because three experimental conditions were available while only two were available for sites B and C). The final objective is indeed to apply the chemical model described here within larger hydrology/sedimentation model, and a single parameter set for a given site is likely to be more useful in this perspective.

3 Results and discussion

3.1 Experimental kinetics of Pb concentrations in water

The evolution of Pb concentrations in the dissolved phase during the resuspension experiments is shown in Figure 3. It showed two stages, whatever the sediment used and the amount of suspended sediments: a first desorption stage, followed by a readsorption stage. The dissolved concentrations increased during the first 5 hours of the experiments for sediment A, 24 h to 48 h for site B, and 5 h to 15 h for site C, followed by a continuous decrease. The maximum concentrations of Pb measured during the experiments were between 2.30 10^{-6} $g.L^{-1}$ (site 'C- 2.1

g.L^{-1}') and 1.37 10^{-5} g.L^{-1} (site 'B- 5.3 g.L^{-1}'). The concentrations of dissolved Pb represent a release of 0.4 to 1.8 % of the total Pb associated to the suspended solid particles.

3.2 Physico-chemical parameters in water

The concentrations of dissolved organic carbon (DOC, not shown – see Monnin et al, 2018 and Monnin 2018) in water during the resuspension experiments ranged between 1 and 5.6 mg.L^{-1} for site A, 2.1 and 7.7 mg.L^{-1} for site B, and 5.5 and 7.9 mg.L^{-1} for site C, depending on the experiments. These variation ranges are wide, however the DOC do not show any clear trend over the duration of the experiments.

The redox potential (Eh) of the stirred and aerated water decreases immediately when sediments are resuspended (results not shown – see Monnin et al, 201 and Monnin 2018). Eh then rises sharply for a short period (up to one hour for site A; Monnin et al. 2018) and then slowly increases up to the end of the experiments. The redox variations do not affect the dissolved speciation of Pb, which is the trace element we chose to model.

The pH follows a similar pattern with an instantaneous decrease after the sediment addition followed by an increase from 10 minutes of resuspension (Figure 4). A larger decline of pH is measured during the resuspension of sediments B and C compared to the sediment A. The XRD analysis of the sediments show that, unlike the sediments B and C, the sediment from site A contains carbonate minerals (calcite and dolomite), of which dissolution have partially buffered the pH decrease.

3.3 Evolution of f_{SO^-} f_{HS^-} and f_{free} during the sediment resuspension

3.3.1 Speciation of the POC and oxides surfaces

418 The total concentrations of oxides and POC in the suspended particles, respectively obtained from the ascorbate extraction and the total organic carbon analysis, are given in Table 2. The
420 sediments from sites B and C contain more POC than those from site A (4.8 to 7.9 % versus 1.6-1.8 %). Higher amounts of Fe, Mn and Al are also extracted in the ascorbate fraction for the
422 sediments B and C, so the concentrations of oxides are higher than for sediment A.

The total concentrations of POC and oxides are assumed to remain constant over the duration of
424 the resuspension experiments. However, the evolution of the physico-chemical conditions during the experiments (ex. pH, ionic strength) may alter the speciation of oxides and POC surfaces and
426 change the concentrations of adsorption sites over time. Cappuyns et al (2014) and Camino Martin-Torre et al (2017) for example shown that the variation of pH associated to changes in
428 oxidation processes during resuspension experiments may had an influence on TM releases. The partition between protonated and deprotonated sites on the POC and Oxides surfaces were
430 calculated according to the models described in 2.4 and the evolution of the fraction of anionic sites (f_{SO^-} and f_{HS^-}) are shown in Figure 5.

432 Both f_{SO^-} and f_{HS^-} follow the same evolution as the pH during the resuspension experiments: a decrease during the first 10 minutes, then an increase. The highest and lowest fractions f_{SO^-} and
434 f_{HS^-} respectively correspond to the resuspension experiments of sediment 'A 5 $g.L^{-1}$' and sediment 'B 5.3 $g.L^{-1}$', during which the highest and lowest pH values are measured. Given the
436 protonation/deprotonation of the surface sites that are considered, the fractions of anionic sites f_{SO^-} and f_{HS^-} are highly dependent of the pH variations. Indeed, a shift in pH influences the
438 direction of the reactions $SOH \rightleftharpoons SO^- + H^+$ and $SHH \rightleftharpoons HS^- + H^+$. According to Le Chatelier's principle, a decrease of pH (increase of $[H^+]$) promotes the formation of *SOH* and
440 *SHH* and the decrease of the fractions of reactive sorption sites SO^- and HS^-.

Decrease (respectively increase) in pH will then decrease (respectively increase) reactive (negatively charged) sites of the oxides and POC. Thus, decrease in pH will decrease the variables f_{SO^-} and f_{HS^-} involved in the reactions

$$f_{free}.M_{dis} + f_{SO^-}.Ox \underset{k_{des,ox}}{\overset{k_{ads,ox}}{\rightleftharpoons}} M_{ox}$$

and

$$f_{free}.M_{dis} + f_{HS^-}.POC \underset{k_{des,POC}}{\overset{k_{ads,POC}}{\rightleftharpoons}} M_{POC}$$

If we consider the Le Chatelier's principle, then each reaction will be directed to counteract the decrease in $f_{SO^-}.Ox$ and $f_{HS^-}.POC$. Each reaction will then be directed in the reverse way.

3.3.2 Speciation of dissolved Pb

The results of speciation calculations show that the vast majority of dissolved Pb is complexed with the dissolved organic matter (data not shown). The free ionic species Pb^{2+} represent only a small fraction of the total amount of dissolved Pb (Figure 5). Minimum f_{free} ($7.0\ 10^{-7}$–$3.8\ 10^{-6}$) are obtained with the input data of resuspension 'A-2.7 $g.L^{-1}$'. The highest calculated f_{free} ($8.6\ 10^{-6}$–$8.4\ 10^{-5}$) correspond to the resuspension 'B-5.3 $g.L^{-1}$'. Over the duration of resuspension, the f_{free} ratios increase up to their highest values during the first 10 minutes and then decrease until the end of the experiments.

During the sediment resuspension, the dissolved Pb remains mainly complexed with the dissolved organic substances but the pH decrease at the beginning of the experiments promotes the increase of the fraction Pb^{2+} (Figures 3 and 5).

The significant kinetic changes in reactive adsorption sites and free metal concentrations during the resuspension experiments, as shown in Figure 5, highlight the importance of taking into

462 account the speciation of Oxides and POC surfaces and the speciation of dissolved TM in the model.

464 **3.4 Carbonate dissolution parameters**

As described in the Material and Method section, the kinetic rate describing carbonate 466 dissolution $k_{dis,carb}$ and the correction factor $\alpha_{dis,carb}$ were calibrated using kinetic evolution of Ca^{2+} and CO_3^{2}, integrated in the Saturation Index of calcite *SI*. Parameter values obtained for the 468 three resuspension experiments with sediments from site A are reported in Table 3.

For the resuspension of the sediments from sites B and C (that do not contain carbonate minerals 470 detected by the XRD analysis), the evolution of alkalinity over time is optimally reproduced by taking into account the pH variation over time only (data not shown). For these resuspension 472 experiments, considering carbonate dissolution did not improve the model results and no kinetic rates of carbonate dissolution were therefore calibrated.

474 The comparison between experimental and calculated SI for the resuspension of sediment A are reported in Figure 4. The dashed blue line represents the SI computed without calcite dissolution, 476 taking into account only pH variations that influence the concentration of CO_3^{2-}. For this site, the pH evolution allows to explain in part the evolution of SI during the experiments, especially 478 during the first hour of resuspension. However, pH variations are not enough to explain the increase of the calcite SI at the end of the three experiments (Figure 4). Adding the process of 480 calcite dissolution, thanks to the calibrated constants $k_{dis,carb}$ and $\alpha_{dis,carb}$, allows the calculated SI to be well adjusted to the measured one. The TM bound to the carbonate fraction in the sediment 482 A before resuspension (deduced from sequential extraction) are then released in the dissolved phase with the same kinetic rate that the calcite dissolution.

484

3.5 Adsorption/desorption parameters on/from oxides and POC

As described in the Material and Method section, the kinetic rates describing adsorption on oxides and POC ($k_{ads,ox}$ and $k_{ads,POC}$) and desorption from oxides and POC ($k_{des,ox}$ and $k_{des,POC}$) were calibrated from experimental data. Parameter values obtained for each of the resuspension experiments are reported in Table 3.

The comparison between measured Pb concentrations (experimental) and calculated concentrations is reported in Figure 3. The goodness-of-fit is in part quantified by the determination coefficient R^2 that is reported in Table 3 for each condition. All the R^2 values are high, characterizing accurate calibration. The calibration of the kinetic rates of adsorption and desorption of Pb at the surface of POC and Oxides, and of the calcite dissolution for site A, allows to faithfully reproduce the kinetic evolution of dissolved Pb during the resuspension of the sediments from the three sites. Besides, uncertainty margins derived from the application of Probability Density Functions for each parameter are narrow, showing the robustness of the modeling approach (Table . The concentrations of Pb increase during the first part of the experiments and then decrease until the end. They reach their maximum values after 5 h with the sediments from site A, 24 to 48 h for site B, and 5 h à 15 h for site C. The release and uptake of Pb over time and the maximum concentration values are well reproduced with the model.

The Pb evolution is successfully reproduced considering its release from one type of solid phase (the oxides pool), added to the release from carbonates in the case of site A, followed by its uptake by another type of solid particles (the organic particulate pool). The values of the calibrated kinetic constants of Pb desorption from oxides ($k_{des,ox}$) are very similar between the experiments for the three sites. The mean values (of the normal distributions indicated in Table 3) of $k_{des,ox}$ ranged from $1.4.10^{-2}$ h^{-1} for site 'C-4.9 $g.L^{-1}$' to $4.5\ 10^{-2}$ h^{-1} for site 'B-1.6 $g.L^{-1}$'. The kinetic constant of adsorption to the oxides $k_{ads,ox}$ is not a sensitive parameter for the modelling of the Pb partition between solid and liquid phase. This is the reason why no PDF was determined for the $k_{ads,ox}$ parameter, but only an extremum value (Table 3). This may be

explained by the assumptions chosen for the model: Pb is indeed assumed to be first released from weak and fast sites present on oxides, and then to be potentially uptaken to slower and stronger POC sites. Readsorption is then dominated by the adsorption kinetic on POC sites and adsorption kinetics on oxides) is then poorly sensitive on modeling results. The kinetic release of dissolved Pb by desorption or dissolution from the oxides is therefore reproduced almost identically between the experiments, while the reverse process of uptake by adsorption or co-precipitation on the oxides is negligible.

The readsorption of dissolved Pb from the solution on the long term is reproduced through the adsorption on the second type of solid phase: the organic particles (POC). The adsorption kinetic rate ($k_{ads,POC}$) showed a greater variability between the three sites, and also between the experiments with the various mass of suspended sediment from a single site (variation by one order of magnitude). For the site A, the adsorption rate of Pb on the POC is similar for the 2.7 and 5.0 $g.L^{-1}$ experiments (respectively 3.9 10^7 and 2.3 10^7 $L.g^{-1}.h^{-1}$) and slightly decreases for the 9.4 $g.L^{-1}$ experiment (7.9 10^6 $L.g^{-1}.h^{-1}$). For the sites B and C, the values of $k_{ads,POC}$ are higher for the experiments with 5.3 and 4.9 $g.L^{-1}$ of suspended sediments than with 1.6 and 2.3 $g.L^{-1}$, showing a potential effect of the solid-to-liquid ratio on adsorption kinetics on strong and slow sites present on POC. Instead, desorption kinetic rates from POC ($k_{des,POC}$) remain quite similar for a given site (range from $2.7.10^{-3}$ to $4.7.10^{-3}$ h^{-1} for site A; from $9.4.10^{-4}$ to $5.9.10^{-3}$ h^{-1} for site B; from $8.3.10^{-3}$ to $1.5.10^{-2}$ h^{-1} for site C), with an inter-site variability over about one order of magnitude. The kinetic readsorption of dissolved lead by uptake to POC sites showed then a slight effect of the solid-to-liquid ratio and a slight inter-site variability. Ranges of variation of the adsorption and desorption kinetic rates related to POC remain however relatively limited (they do not exceed one order of magnitude), considering the fact that sediments originated from quite contrasted reservoirs.

As indicated in section 2.8, a single set of parameter PDFs was also calibrated by considering the three experimental conditions tested for site A together. Parameter PDFs thus obtained are presented in Table 3, as well as the determination coefficient R^2 (indicator of the goodness-of-fit). The model goodness-of-fit thus obtained is unavoidably poorer than those obtained by separate calibration (0.78 for the 'all-together' calibration versus 0.97, 0.94 and 0.94 for the 'single' calibrations), but it remains quite acceptable, showing that a global calibration is of good value for a further incorporation within a larger hydrology/sedimentation model.

4 Conclusion

This study evidenced the interest of 'long-term' experiments for a better characterisation of the interactions of Pb between water and sediments in the context of resuspension events. Such experiments showed that exchanges of Pb between sediments and water can efficiently be represented by multi-compartmental kinetic model. This model is innovative since it combines thermodynamic speciation of particulate surfaces (oxides and POC), thermodynamic TM speciation in water, and kinetic modelling of exchanges between free TMs and particulate sites.

Uptake and release processes were found to be controlled by at least two successive (fast and slow) reactions that can be associated to two particulate pools (here oxides and POC). The relative contribution of fast and slow reactions respectively on the partitioning at the water-particles interface was quantified for different contexts (three sites and different sediment concentrations) through the calibration of kinetic adsorption and desorption rates. Variability in kinetic rates allowed to evaluate the effect of solid-to-liquid ratio and sediment origin on exchange kinetics at the water-particles interface. It was shown that the kinetic release of dissolved Pb by desorption or dissolution from the oxides is reproduced almost identically between the experiments, regardless solid-to-liquid ratio and sediment origin. Readsorption on

the long term on POC sites is more variable, even if ranges of variation in the adsorption and desorption kinetic rates related to POC remain limited considering that tested sediments are quite contrasted.

When simulating the behaviour of a TM like Pb in a reservoir submitted to resuspension events, it is therefore necessary to take into account several exchange processes and the residence time of the particulate phase downstream to the resuspension point. The model described in this paper is able to simulate transient processes and modification in the speciation of particulate TMs. It would be interesting to compare chemical time constants determined in this paper with the residence time of water and particles downstream to reservoirs. Consequently, to know whether chemical kinetics play a major role on the behavior of TMs during their downstream transit, it would be useful to combine the chemical model developed in this paper with hydraulic and sedimentological models.

571 **References**

572 Anschutz, P., Zhong, S., Sundby, B., Mucci, A., Gobeil, C. (1998). Burial efficiency of
573 phosphorus and the geochemistry of iron in continental margin sediments. Limnology and
574 Oceanography, 43, 53-64. https://doi.org/10.4319/lo.1998.43.1.0053

575 Caetano, M., Madureira, M.-J., Vale, C. (2003). Metal remobilisation during resuspension of
576 anoxic contaminated sediment: short-term laboratory study. Water, Air and Soil Pollution 143, 23–
577 40. https://doi.org/10.1023/A:1022877120813

578 Caille, N., Tiffreau, C., Leyval, C., Morel, J.L. (2003). Solubility of metals in an anoxic
579 sediment during prolonged aeration. Science of The Total Environment 301, 239–250.
580 https://doi.org/10.1016/S0048-9697(02)00289-9

581 Camino Martin-Torre M., Cifrian E., Ruiz G., Galan B., Viguri J.R. (2017). Estuarine sediment
582 resuspension and acidification : release behaviour of contaminants under different oxidation levels
583 and acid sources. Journal of environmental Management. 199, 211-221.
584 http://dx.doi.org/10.1016/jenvman.2017.05.044

585 Cantwell, M.G., Burgess, R.M., Kester, D.R. (2002). Release and phase partitioning of metals
586 from anoxic estuarine sediments during periods of simulated resuspension. Environmental Science
587 and Technology 36, 5328-5334. https://doi.org/10.1021/es0115058

588 Cappuyns, V., Alian, V., Vassilieva, E., & Swennen, R. (2014). pH dependent leaching
589 behavior of Zn, Cd, Pb, Cu and As from mining wastes and slags: kinetics and mineralogical control.
590 *Waste and Biomass Valorization*, *5*(3), 355-368

591 Ciffroy, P., Garnier, J.-M., Khanh Pham, M. (2001). Kinetics of the adsorption and desorption
592 of radionuclides of Co, Mn, Cs, Fe, Ag and Cd in freshwater systems: experimental and modelling
593 approaches. Journal of Environmental Radioactivity, 55, 71–91. https://doi.org/10.1016/S0265-
594 931X(01)00026-1

595 Ciffroy, P., Garnier, J.-M., Benyahya, L. (2003). Kinetic partitioning of Co, Mn, Cs, Fe, Ag, Zn
596 and Cd in fresh waters (Loire) mixed with brackish waters (Loire estuary): experimental and
597 modelling approaches. Marine Pollution Bulletin, 46, 626–641. https://doi.org/10.1016/S0025-
598 326X(02)00517-9

599 Ciffroy, P., Nia, Y., Garnier, J.M. (2011). Probabilistic multicompartmental model for
600 interpreting DGT kinetics in sediments. Environmental science and technology, 45, 9558-9565.
601 https://doi.org/10.1021/es104221b

602 Ciffroy, P., Alfonso, B., Altenpohl, A., Banjac, Z., Bierkens, J., Brochot, C., Critto A, De
603 Wilde T., Fait G., Fierens T., Garratt J., Giubilato E., Grange E., Johansson E., Radomyski A.,
604 Reschwann K., Suciu N., Tanaka T., Tedoisi A., Van Holderbeke M., Verdonck F. (2016). Modelling
605 the exposure to chemicals for risk assessment: a comprehensive library of multimedia and PBPK
606 models for integration, prediction, uncertainty and sensitivity analysis–the MERLIN-Expo tool.
607 Science of the Total Environment, 568, 770-784. https://doi.org/10.1016/j.scitotenv.2016.03.191

608 Ciffroy, P., & Benedetti, M. (2018). A comprehensive probabilistic approach for integrating
609 natural variability and parametric uncertainty in the prediction of trace metals speciation in surface
610 waters. *Environmental pollution*, *242*, 1087-1097

611 De Jonge, M., Teuchies, J., Meire, P., Blust, R., & Bervoets, L. (2012). The impact of increased
612 oxygen conditions on metal-contaminated sediments part I: Effects on redox status, sediment
613 geochemistry and metal bioavailability. *Water research*, *46*(7), 2205-2214

614 Dzombak, D.A., Morel, F.M.M. (1990). Surface complexation modelling: hydrous ferric oxide.
615 Wiley-Interscience, New York

616 Ferdelman, T.G. (1988) The distribution of sulfur, iron, manganese, copper and uranium in salt
617 marsh sediment cores as determined by sequential extraction methods. Dissertation, University of
618 Delaware

Garnier, J.-M., Ciffroy, P., Benyahya, L. (2006). Implications of short and long term (30 days) sorption on the desorption kinetic of trace metals (Cd, Zn, Co, Mn, Fe, Ag, Cs) associated with river suspended matter. Science of The Total Environment, 366, 350–360. https://doi.org/10.1016/j.scitotenv.2005.07.015

Gustafsson, J.P. (2001). Modeling the acid-base properties and metal complexation of humic substances with the Stockholm Humic Model. Journal of Colloid and Interface Science, 244, 102-112. https://doi.org/10.1006/jcis.2001.7871

Gustafsson, J. P., Berggren Kleja, D. (2005). Modeling salt-dependent proton binding by organic soils with the NICA-Donnan and Stockholm Humic models. Environmental Science and Technology, 39, 5372-5377.

Hwang, K.-Y., Kim, H.-S., Hwang, I. (2011). Effect of resuspension on the release of heavy metals and water chemistry in anoxic and oxic sediments. CLEAN Soil Air Water, 39, 908–915. https://doi.org/10.1002/clen.201000417

Iman, R.L., Conover, W.J. (1982). A distribution-free approach to inducing rank correlation among input variables. Community Statistical Simulation Computation, 11, 311-334.

Kalnejais, L.H., Martin, W.R., Bothner, M.H. (2010). The release of dissolved nutrients and metals from coastal sediments due to resuspension. Marine Chemistry, 121, 224–235. https://doi.org/10.1016/j.marchem.2010.05.002

Kostka, J.E., Luther, G.W. (1994). Partitioning and speciation of solid phase iron in saltmarsh sediments. Geochimica Cosmochimica Acta, 58, 1701-1710. https://doi.org/10.1016/0016-7037(94)90531-2

MacDonald, D.D., Ingersoll, C.G., Berger, T.A. (2000) Development and evaluation of consensus-based sediment quality guidelines for freshwater ecosystems. Archives of Environmental Contamination and Toxicology, 39, 20-3. https://doi.org/10.1007/s002440010075

643 Monnin, L., Ciffroy, P., Garnier, J. M., Ambrosi, J. P., & Radakovitch, O. (2018).
644 Remobilization of trace metals during laboratory resuspension of contaminated sediments from a
645 dam reservoir. *Journal of Soils and Sediments*, *18*(7), 2596-2613.https://doi.org/10.1007/s11368-018-
646 1931-5Monnin L. (2018) Changement de speciation des éléments traces métalliques lors de la remise
647 en suspension de sédiments de barrages. PhD Aix-Marseille University, 183 pp.

648 Nia, Y., Garnier, J. M., Rigaud, S., Hanna, K., Ciffroy, P. (2011). Mobility of Cd and Cu in
649 formulated sediments coated with iron hydroxides and/or humic acids: a DGT and DGT-PROFS
650 modeling approach. Chemosphere, 85, 1496-1504.
651 https://doi.org/10.1016/j.chemosphere.2011.08.045

652 Poupart, M., Royet, P. (2001). La surveillance des grands barrages. Colloque Technique du
653 Comité Français des Barrages et Réservoirs, Aix-en-Provence.

654 Quevauviller, P. (2007). Fractionnement d'éléments pour étude dans l'environnement.
655 Techniques de l'ingénieur, pp 3854.

656 Rauret, G. (1998). Extraction procedures for the determination of heavy metals in contaminated
657 soil and sediment. Talanta, 46, 449-455. https://doi.org/10.1016/S0039-9140(97)00406-2

658 Saulnier, I., Mucci, A. (2000). Trace metal remobilization following the resuspension of
659 estuarine sediments: Saguenay Fjord, Canada. Applied Geochemistry, 15, 191–210.
660 https://doi.org/10.1016/S0883-2927(99)00034-7

661 SedNet, European Sediment Research Network (2004). Contaminated sediments in European
662 river basins. 69p.

663 Simpson, S.L., Apte, S.C., Batley, G.E. (2000). Effect of Short-Term Resuspension Events on
664 the Oxidation of Cadmium, Lead, and Zinc Sulfide Phases in Anoxic Estuarine Sediments. Environ.
665 Sci. Technol. 34, 4533–4537. https://doi.org/10.1021/es991440x

666 Superville, P.-J., Prygiel, E., Magnier, A., Lesven, L., Gao, Y., Baeyens, W., Ouddane, B.,
667 Dumoulin, D., Billon, G. (2014). Daily variations of Zn and Pb concentrations in the Deûle River in

668 relation to the resuspension of heavily polluted sediments. Science of The Total Environment, 470–
669 471, 600–607. https://doi.org/10.1016/j.scitotenv.2013.10.015

670 Tessier, A., Campbell, P.G.C., Bisson, M. (1979). Sequential extraction procedure for the
671 speciation of particulate trace metals. Analytical Chemistry, 51, 844–851.
672 https://doi.org/10.1021/ac50043a017

673 Tipping, E. (1998). Humic ion-binding model VI: an improved description of the interactions
674 of protons and metal ions with humic substances. *Aquatic geochemistry*, *4*(1), 3-47

675 Ye, S., Laws, E.A., Gambrell, R. (2013). Trace element remobilization following the
676 resuspension of sediments under controlled redox conditions: City Park Lake, Baton Rouge, LA.
677 Applied Geochemistry 28, 91–99. https://doi.org/10.1016/j.apgeochem.2012.09.008

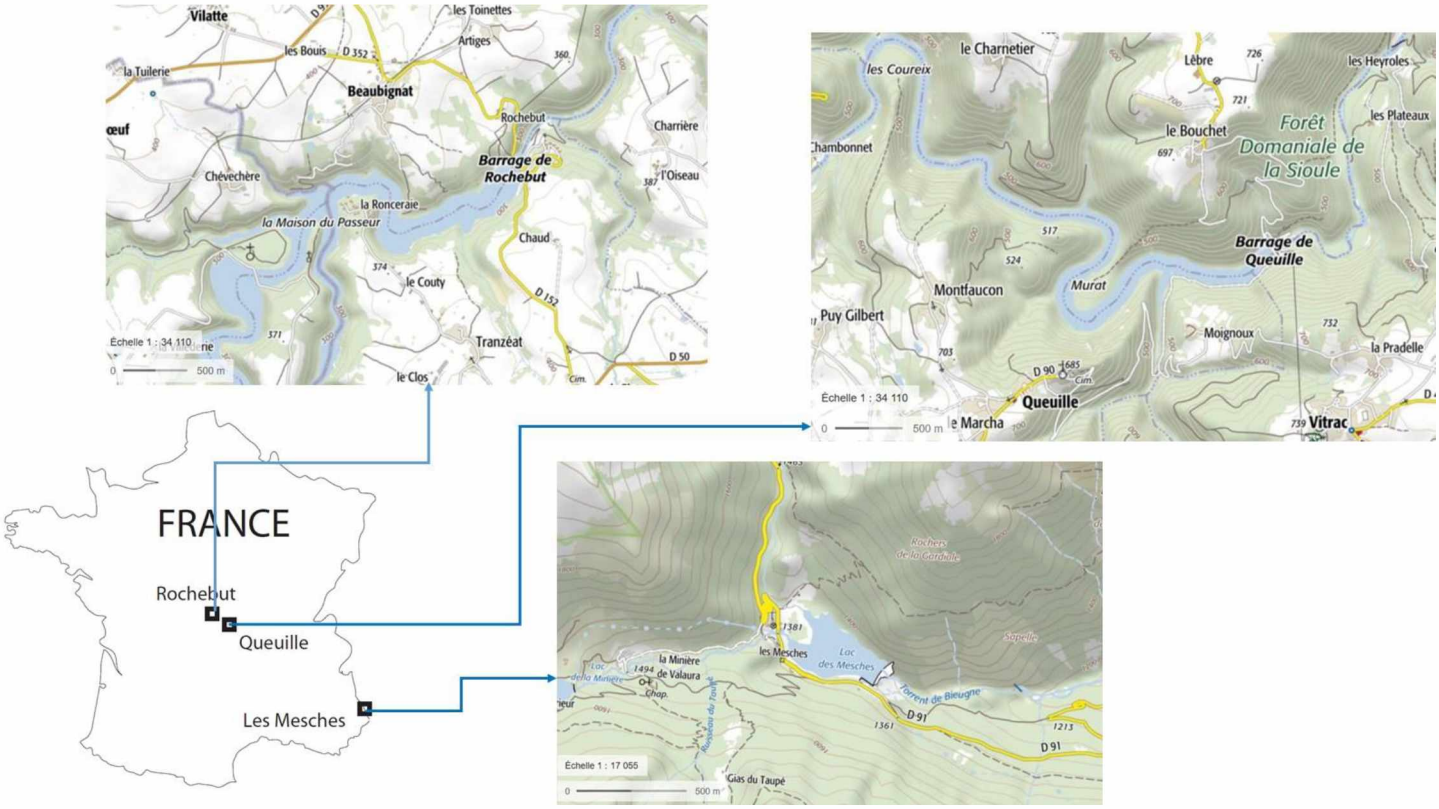

Figure 1 - Locality map showing the 3 sites in relation to France and detailed locality maps

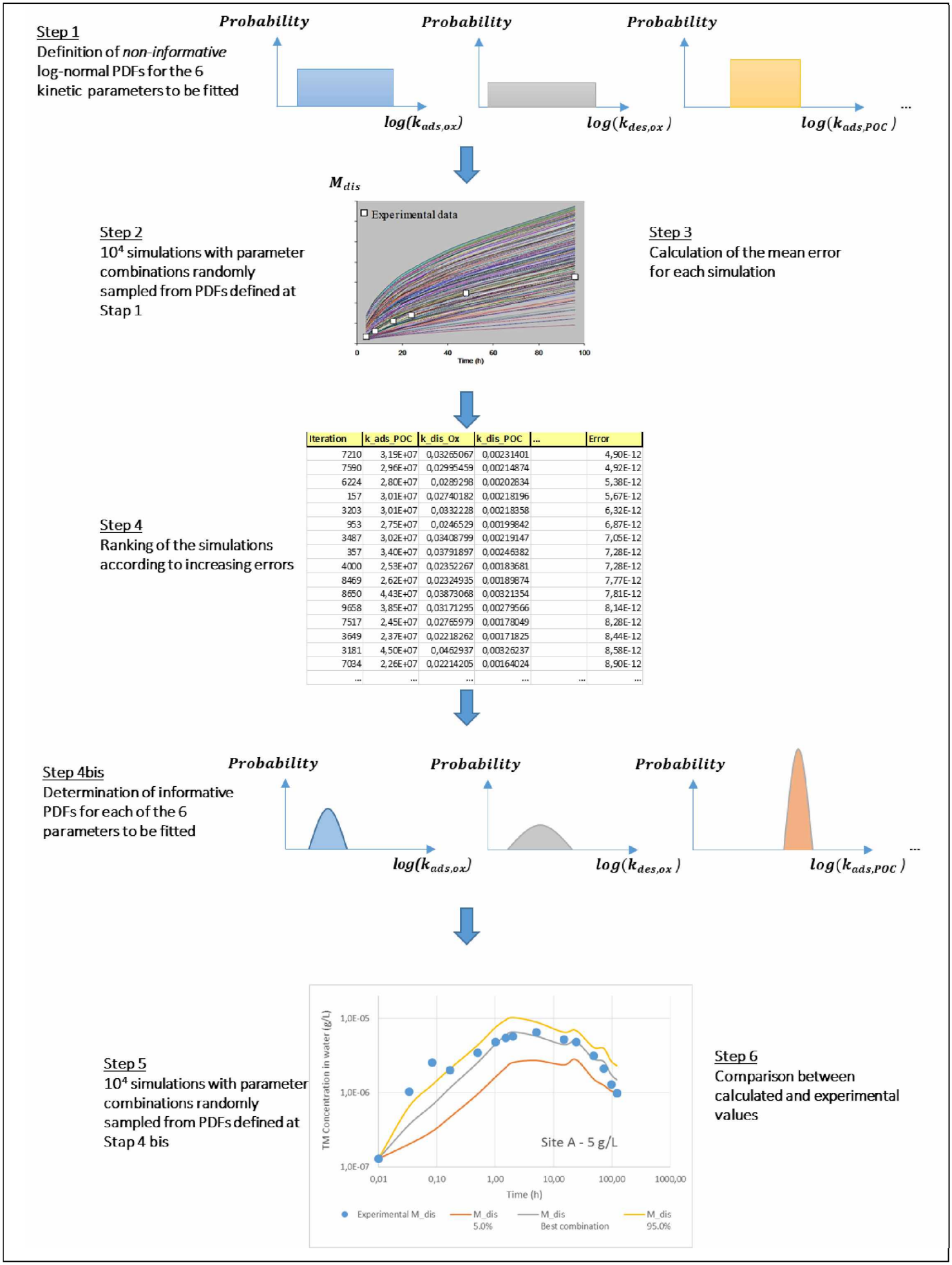

Iteration	k_ads_POC	k_dis_Ox	k_dis_POC	...	Error
7210	3,19E+07	0,03265067	0,00231401		4,90E-12
7590	2,96E+07	0,02995459	0,00214874		4,92E-12
6224	2,80E+07	0,0289298	0,00202834		5,38E-12
157	3,01E+07	0,02740182	0,00218196		5,67E-12
3203	3,01E+07	0,0332228	0,00218358		6,32E-12
953	2,75E+07	0,0246529	0,00199842		6,87E-12
3487	3,02E+07	0,03408799	0,00219147		7,05E-12
357	3,40E+07	0,03791897	0,00246382		7,28E-12
4000	2,53E+07	0,02352267	0,00183681		7,28E-12
8469	2,62E+07	0,02324935	0,00189874		7,77E-12
8650	4,43E+07	0,03873068	0,00321354		7,81E-12
9658	3,85E+07	0,03171295	0,00279566		8,14E-12
7517	2,45E+07	0,02765979	0,00178049		8,28E-12
3649	2,37E+07	0,02218262	0,00171825		8,44E-12
3181	4,50E+07	0,0462937	0,00326237		8,58E-12
7034	2,26E+07	0,02214205	0,00164024		8,90E-12
...	...	...	...	...	...

Figure 2 - Steps followed for fitting model parameters

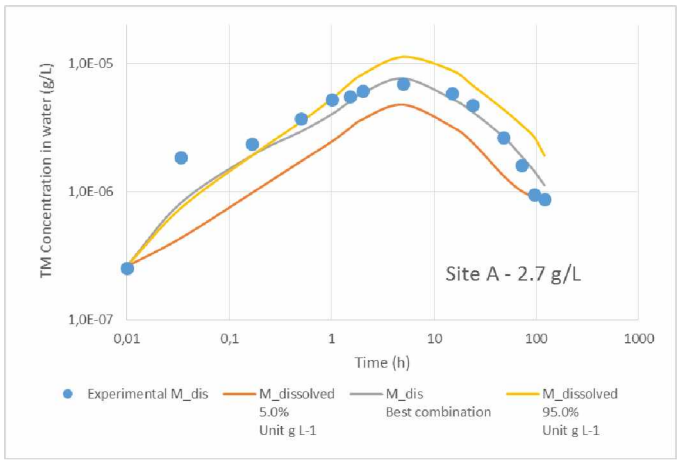

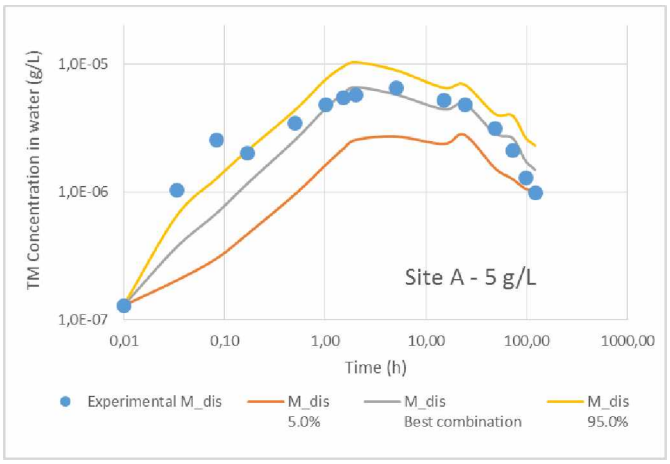

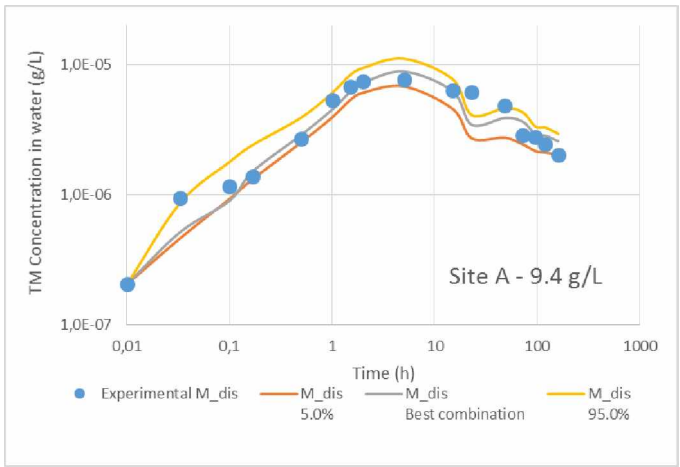

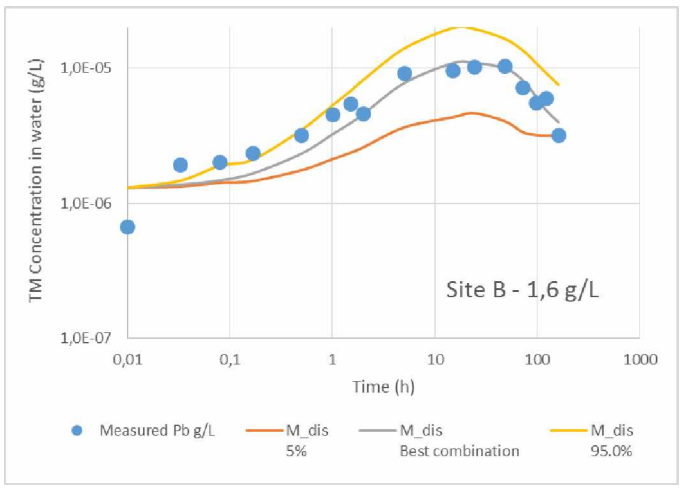

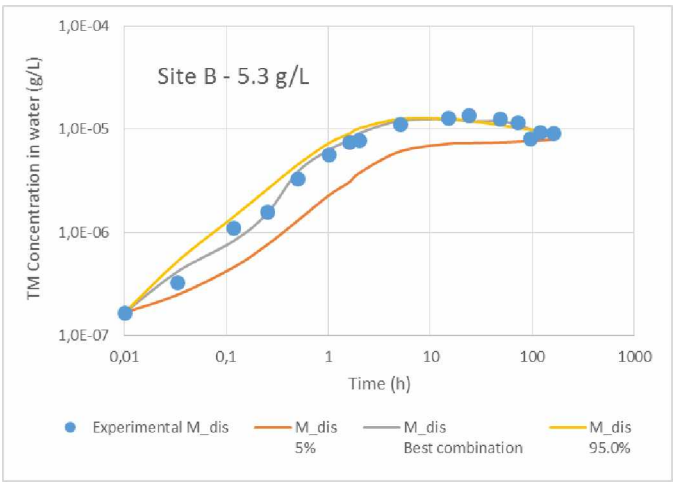

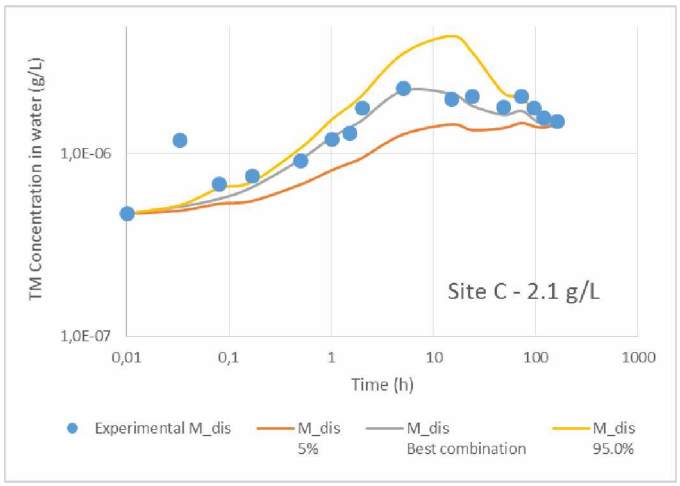

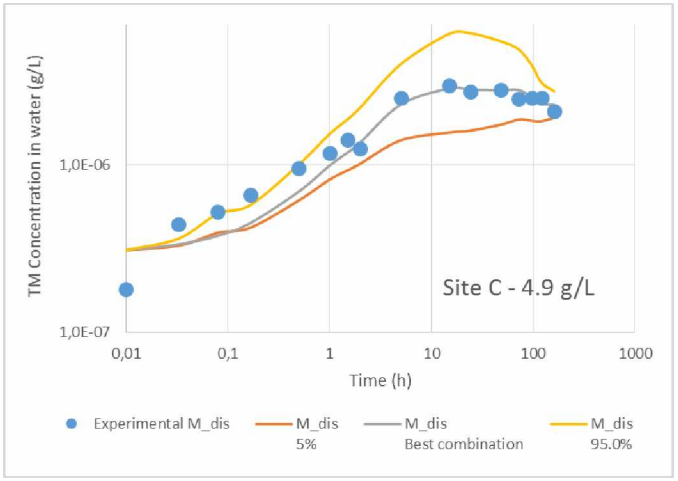

Figure 3 – Dissolved Pb concentration – Comparison between experimental (blue dots) and calculated kinetic evolutions (best combination of parameters, 5th percentile and 95th percentile of the curves generated with the PDFs obtained for each of the parameters)

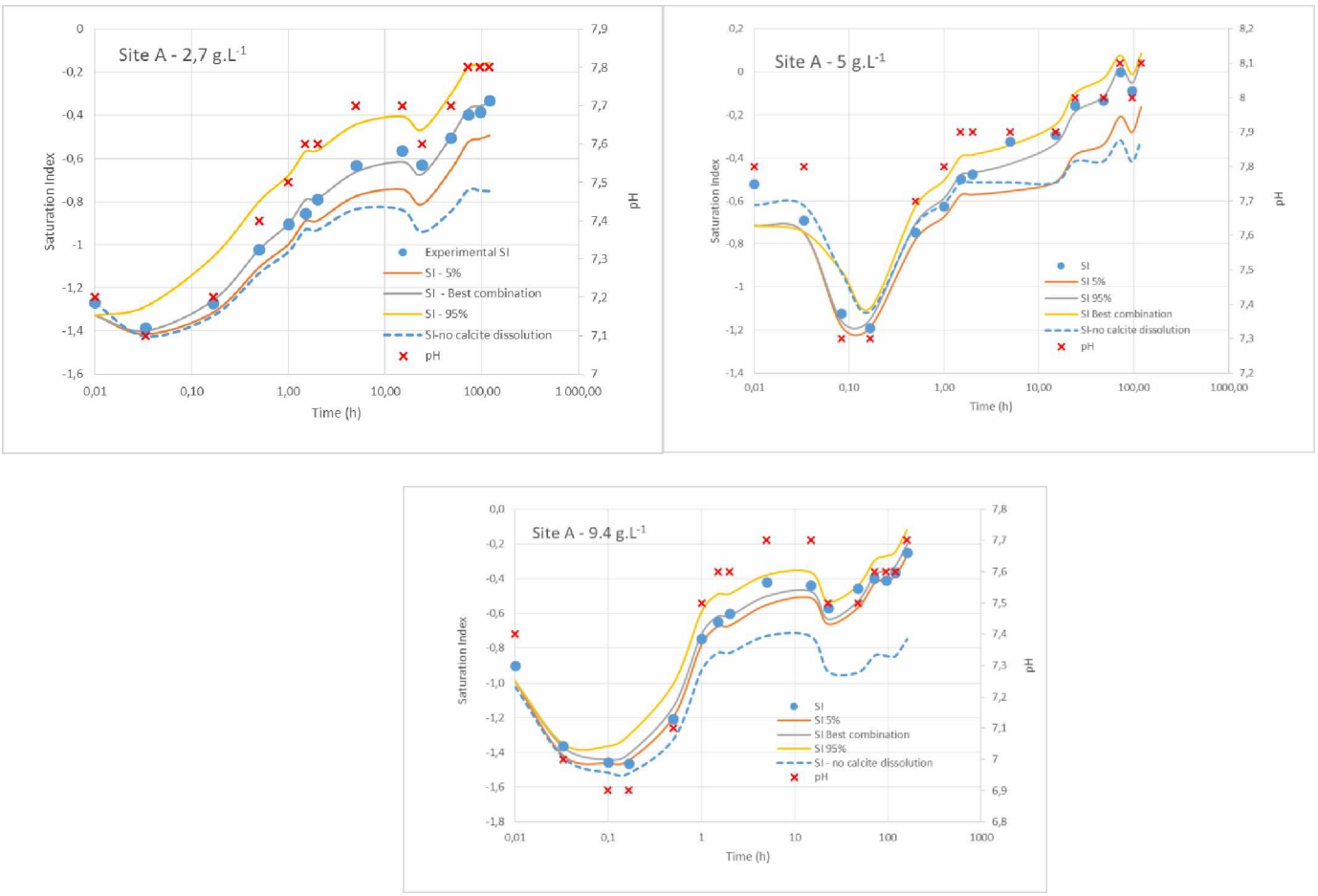

Figure 4 – Saturation index (SI) of calcite – Comparison between experimental and calculated kinetic evolutions. The dashed blue line represents the SI computed without calcite dissolution

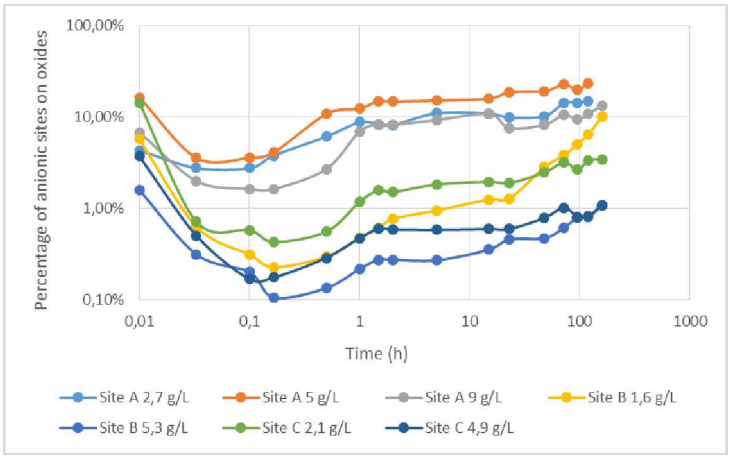

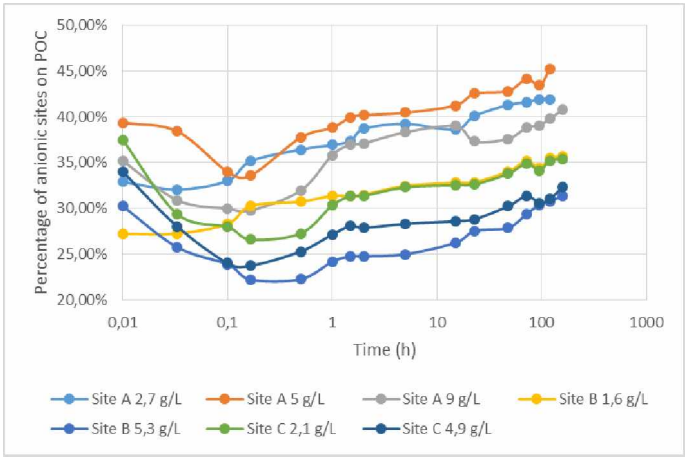

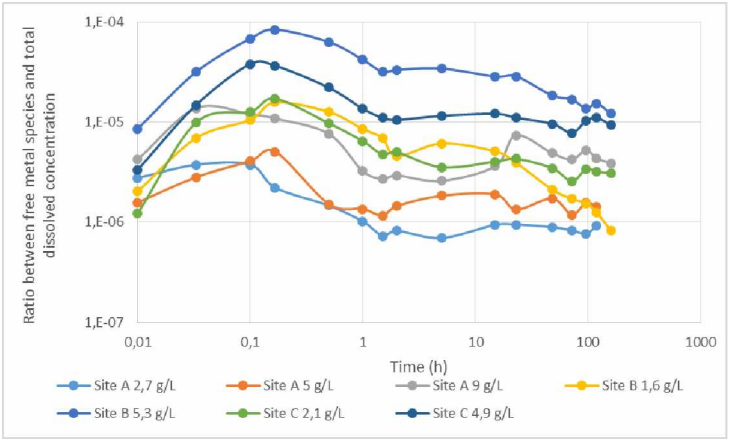

Figure 5 – Fraction of anionic sites f_{SO-} (%, log scale) on the surface of oxides, fraction of anionic sites f_{HS-} (%) on the surface of POC, and Ratio f_{free} between free species Pb^{2+} and the total dissolved concentration during the resuspension experiments, for the three sites and all the resuspension experiments.

Simulated process	Aim of the sub-model	Equilibrium[1] vs Kinetic[2] assumption	Parameters involved in the model	Source and Reference
Speciation of oxide surfaces	Calculating the distribution of deprotonated (SO^-), neutral (SOH) and protonated species (SOH_2^+) on oxide surface	Equilibrium assumption	Physico-chemical characteristics of hydrous ferric oxides: • Specific Surface Area of oxide, SSA_{SOH} • Density of monodentate binding sites, $Site\_density_{S1}$ • Density of multidentate binding sites, $Site\_density_{S2}$ Equilibrium constant of protonation/deprotonation reactions • Equilibrium constant of reaction S1OH ↔ $S1O^-$, $logK_{S1O-}$ • Equilibrium constant of reaction S1OH ↔ $S1OH_2^+$, $logK_{S1OH2+}$ • Equilibrium constant of reaction S2OH ↔ $S2O^-$, $logK_{S2OH2+}$ • Equilibrium constant of reaction S2OH ↔ $S2OH_2^+$, $logK_{S2O-}$	'HFO' model from Dzombak and Morel (1990) Parameter values are taken from Dzombak and Morel (1990) and are synthetized in Ciffroy and Benedetti (2018)
Speciation of the POC surface	Calculating the distribution of deprotonated (HS^-) and neutral (HHS) species on the POC surface (Humic substances)	Equilibrium assumption	Physico-chemical characteristics of the Humic Substances (HS): • Site density of functional groups on HS, N_S • Percentage of active DOM that is Fulvic Acids (FA), $Ratio\_FA/DOM$ • Percentage of active Particulate Organic Carbon (POC) that is FA, $Ratio\_FA/POC$ • Group density on FA (quantity of binding sites per unit mass of FA), $Group\_density_{FA}$ • Group density on Humic Acids (HA) (quantity of binding sites per unit mass of HA), $Group\_density_{HA}$ Equilibrium constant of protonation/deprotonation reactions • Intrinsic proton dissociation constants for carboxylic (type A) and phenolic (type B) sites on FA and HA, $logK_{FA\_A}$; $logK_{FA\_B}$; $logK_{HA\_A}$; $logK_{HA\_B}$ (four parameters) • Distribution terms modifying for types A and B of FA and HA, ΔpK_{FA_A}; ΔpK_{FA_B}; ΔpK_{HA_A}; ΔpK_{HA_B} (four parameters) • Gel fraction parameter for dissolved FA and HA, gf_{FAd}; gf_{HAd} • Stern layer capacitance, C	Stockholm Humic Substances Model (SHM) from Gustafsson (2001) Parameter values are taken from Gustafsson (2001)and are synthetized in Ciffroy and Benedetti (2018)
Complexation of TM with inorganic ligands	Calculating the concentration of TM complexed with hydroxyls, nitrates, sulfates, chlorine and carbonates ions, , and then calculating the distribution among free TM (M^{z+}) and complexed species (ML) in solution	Equilibrium assumption	Affinity constants at equilibrium of the reactions between free TM (M^{z+}) and ligand (OH^- or NO_3^- or SO_4^{2-} or Cl^- or CO_3^{2-}) to give complexed species (ML)	Parameter values are taken from Visual Minteq
Complexation of TM with Dissolved Organic Matter (DOM)	Calculating the concentration of TM complexed with DOM, and then calculating the distribution among free TM (M^{z+}) and	Equilibrium assumption	Equilibrium constant of the reaction leading to the formation of monodentate humic substance-TM complex, $logK_{HSM\_mono}$ Equilibrium constant of the reaction leading to the formation of bidentate humic	Stockholm Humic Substances Model (SHM) from Gustafsson (2001)

	complexed species (M-DOM) in solution		substance-TM complex, $logK_{HSM\_bi}$ Distribution term modifying equilibrium constants for humic substances, ΔLK_{HSM}	Parameter values are taken from Gustafsson (2001) and Tipping et al (2011), and are synthetized in Ciffroy and Benedetti (2018)
Speciation of carbonates in solution	Calculating the distribution among CO_3^{2-}, HCO_3^- and H_2CO_3	Equilibrium assumption	Equilibrium constants of the Acid/Base reactions of the HCO_3^-/CO_3^{2-} and H_2CO_3/HCO_3^- couples	Parameter values are taken from Visual Minteq
Dissolution/Precipitation of carbonates + Dissolution/Coprecipitation of TM from/to carbonates	Calculating the kinetics in the dissolution of calcite to carbonates in solution	Kinetic assumption	Dissolution kinetic rate, $k_{dis,carb}$ Solubility product of calcite, K_s Exponential correction factor, $\alpha_{dis,carb}$	This model Calibrated for each experimental condition
Complexation of TM with hydrous oxides	Calculating the kinetic adsorption/desorption of TM to/from oxides	Kinetic assumption	Desorption/dissolution rate constant from oxides, $k_{des,ox}$ Adsoption rate constant to oxides, $k_{ads,ox}$	This model Calibrated for each experimental condition
Complexation of TM with POC	Calculating the kinetic adsorption/desorption of TM to/from POC	Kinetic assumption	Desorption/degradation rate constant from POC, $k_{des,POC}$ Adsoption rate constant to POC, $k_{ads,POC}$	This model Calibrated for each experimental condition

Table 1 – Processes, assumptions and parameters involved in the model

(1) 'Equilibrium' assumption means that all the reactions involved for simulating the targeted process are described by equilibrium constants

(2) 'Kinetic' assumption means that all the reactions involved for simulating the targeted process are described by forward and reverse kinetic rate constants

Site	Sediment conc. $g.L^{-1}$	Oxides concentration $(g.L^{-1})$	POC $(g.L^{-1})$	$k_{dis,carb}$ h^{-1}	$\alpha_{dis,carb}$ unitless	$k_{ads,ox}$ $L.g^{-1}.h^{-1}$	$k_{des,ox}$ h^{-1}	$k_{ads,POC}$ $L.g^{-1}.h^{-1}$	$k_{des,POC}$ h^{-1}	R^2
A	2.7	$8.31\ 10^{-3}$	$4.32\ 10^{-2}$	$\mathcal{N}(1.85.10^{-5}; 1.6.10^{-5})$	$\mathcal{N}(5.94; 1.1)$	$< 10^{6}$	$\mathcal{N}(3.6.10^{-2}; 1.3.10^{-2})$	$\mathcal{N}(3.9.10^{7}; 1.5.10^{7})$	$\mathcal{N}(2.8.10^{-3}; 1.4.10^{-3})$	0.97
	5.0	$1.54\ 10^{-2}$	$8.80\ 10^{-2}$	$\mathcal{N}(2.2.10^{-4}; 1.3.10^{-4})$	$\mathcal{N}(4.25; 0.61)$	$< 10^{6}$	$\mathcal{N}(2.7.10^{-2}; 1.5.10^{-2})$	$\mathcal{N}(2.3.10^{7}; 8.6.10^{6})$	$\mathcal{N}(2.7.10^{-3}; 1.3.10^{-3})$	0.94
	9.4	$2.89\ 10^{-2}$	$1.65\ 10^{-1}$	$\mathcal{N}(1.1.10^{-5}; 8.5.10^{-6})$	$\mathcal{N}(5.46; 0.98)$	$< 10^{6}$	$\mathcal{N}(1.8.10^{-2}; 7.9.10^{-3})$	$\mathcal{N}(7.9.10^{6}; 3.9.10^{6})$	$\mathcal{N}(4.7.10^{-3}; 2.6.10^{-3})$	0.94
	All conditions together			$\mathcal{N}(8.3.10^{-5}; 5.1.10^{-5})$	$\mathcal{N}(5.22; 0.9)$	$< 10^{6}$	$\mathcal{N}(2.45.10^{-2}; 8.10^{-3})$	$\mathcal{N}(2.1.10^{7}; 9.10^{6})$	$\mathcal{N}(1.8.10^{-3}; 1.6.10^{-3})$	0.78
B	1.6	$8.50\ 10^{-2}$	$1.02\ 10^{-1}$	0	-	$< 10^{5}$	$\mathcal{N}(4.5.10^{-2}; 2.1.10^{-2})$	$\mathcal{N}(1.5.10^{6}; 6.7.10^{5})$	$\mathcal{N}(9.4.10^{-4}; 4.1.10^{-4})$	0.96
	5.3	$2.82\ 10^{-1}$	$4.16\ 10^{-1}$	0	-	$< 10^{5}$	$\mathcal{N}(2.3.10^{-2}; 7.4.10^{-3})$	$\mathcal{N}(3.3.10^{5}; 1.3.10^{5})$	$\mathcal{N}(5.9.10^{-3}; 2.3.10^{-3})$	0.98
C	2.1	$8.10\ 10^{-2}$	$1.01\ 10^{-1}$	0	-	$< 10^{5}$	$\mathcal{N}(3.7.10^{-2}; 1.2.10^{-2})$	$\mathcal{N}(4.10^{6}; 1.5.10^{6})$	$\mathcal{N}(1.5.10^{-2}; 5.6.10^{-3})$	0.94
	4.9	$1.89\ 10^{-1}$	$2.38\ 10^{-1}$	0	-	$< 10^{5}$	$\mathcal{N}(1.4.10^{-2}; 4.7.10^{-3})$	$\mathcal{N}(5.6.10^{5}; 2.4.10^{5})$	$\mathcal{N}(8.3.10^{-3}; 3.5.10^{-3})$	0.99

Table 1 – Probability Density Functions (PDFs) of the parameters fitted. PDFs provided in the table are normal PDFs $\mathcal{N}$(mean; SD).